Precisely and accurately localizing single emitters in fluorescence microscopy

Hendrik Deschout[1,2], Francesca Cella Zanacchi[3,4], Michael Mlodzianoski[5], Alberto Diaspro[3,4], Joerg Bewersdorf[6,7], Samuel T Hess[5] & Kevin Braeckmans[1,2]

Methods based on single-molecule localization and photophysics have brought nanoscale imaging with visible light into reach. This has enabled single-particle tracking applications for studying the dynamics of molecules and nanoparticles and contributed to the recent revolution in super-resolution localization microscopy techniques. Crucial to the optimization of such methods are the precision and accuracy with which single fluorophores and nanoparticles can be localized. We present a lucid synthesis of the developments on this localization precision and accuracy and their practical implications in order to guide the increasing number of researchers using single-particle tracking and super-resolution localization microscopy.

One of the major quests in fluorescence microscopy is to image specimens with the highest detail possible. The amount of detail that can be resolved by a conventional light microscope is, however, fundamentally limited by the diffraction of light. Even an infinitely small point source of light is still imaged as a spot of finite volume, known as the point spread function (PSF). Consequently, the PSFs of two point sources that are closer together than the PSF width will show substantial overlap, making it difficult or impossible to distinguish them from one another. Based on the pioneering work by Abbe[1] and Rayleigh[2], the resolution in the focal plane is often approximated as $0.5\lambda/NA$, with λ being the wavelength of light and NA the numerical aperture of the microscope objective lens. The attainable resolution is thus fundamentally limited to around 200 nm for visible light ($\lambda = 550$ nm) using a high-NA objective lens (NA = 1.4). However, when it comes to determining the location of a single, isolated subresolution particle, such as a single fluorophore, this limit is of less importance, as the isolated spot of light coming from this particle does not need to be distinguished from any other structure in the vicinity. Although the spot shape is related to the PSF, the particle's location

can be determined with a precision and accuracy down to the nanometer scale (**Box 1** and **Fig. 1**).

Although this intuitive concept has been known for a long time[3,4], it was not until light detectors became sensitive enough in the 1980s that it was put into practice and applied in a technique generally known as single-particle tracking (SPT). An SPT experiment begins with recording a time series of images of fluorescently labeled subresolution particles that are isolated from each other so that the spots of light coming from the individual particles (i.e., diffraction limited spots of light) are spatially separate. Subsequently, each individual particle spot is identified in every image, and their positions are calculated. This in turn allows users to determine the trajectories of the individual particles, which can be used for further analysis. As SPT was applied to various systems, it was soon realized that knowledge of the precision and accuracy with which the position of a single fluorescent particle can be estimated was of vital importance for correct analysis of the particle trajectories: for example, for the determination of the diffusion coefficient from Brownian motion trajectories[5].

The interest in localization precision and accuracy has recently increased considerably owing to the development of super-resolution microscopy

[1]Laboratory of General Biochemistry and Physical Pharmacy, Ghent University, Ghent, Belgium. [2]Center for Nano- and Biophotonics, Ghent University, Ghent, Belgium. [3]Department of Nanophysics, Italian Institute of Technology, Genoa, Italy. [4]Department of Physics, University of Genoa, Genoa, Italy. [5]Department of Physics and Astronomy, University of Maine, Orono, Maine, USA. [6]Department of Cell Biology, Yale University School of Medicine, New Haven, Connecticut, USA. [7]Department of Biomedical Engineering, Yale University, New Haven, Connecticut, USA. Correspondence should be addressed to K.B. (kevin.braeckmans@ugent.be).

REVIEW

techniques based on localizing individual fluorophores, such as photoactivated localization microscopy (PALM)[6], fluorescence PALM (FPALM)[7] and stochastic optical reconstruction microscopy (STORM)[8]. Key to these techniques is the consecutive on- and off-switching of fluorophores within a spectral detection window[9]. The imaging procedure starts with the fluorophores in an off (dark) state, either by using fluorescent proteins that are natively expressed in an off state[6,7] or by using fluorophores that are converted into an off state by a suitable illumination procedure[8]. Next, a random but sparse subset of fluorophores is activated through illumination of the sample with light of suitable wavelength and intensity. This subset is then imaged by light of an

---

BOX 1 THE CONCEPT OF LOCALIZATION PRECISION AND ACCURACY

The position coordinates (x_p, y_p, z_p) of an isolated fluorescent emitter can be estimated from a microscopy image with a limited certainty that comprises both a precision and an accuracy (**Fig. 1**). If the true position coordinate x_p of a particle is measured multiple times, the localization precision describes the spread of these estimates $x_{p,i}$ around its mean value $\bar{x}_p$, whereas the localization accuracy describes the deviation of the mean of the measured position coordinates $\bar{x}_p$ from the true position coordinate x_p.

Commonly expressed in terms of a standard deviation σ_x, the localization precision can be determined as

$$\sigma_x = \sqrt{\frac{1}{n-1}\sum_{i=1}^{n}(x_{p,i} - \bar{x}_p)^2}$$

where n is the number of estimates. Sometimes, the localization precision is represented by the full-width at half-maximum FWHM_x of the distribution of measured position coordinates $x_{p,i}$, which is related to the standard deviation representation σ_x as

$$\text{FWHM}_x = 2\sqrt{2\ln 2}\,\sigma_x$$

Similar expressions of the localization precision hold for the position coordinates y_p and z_p.

The localization precision is essentially determined by the photons that make up the image. The number of photons arriving in a certain time interval follows a Poisson distribution, the standard deviation of which is known as shot noise. The photon positions have a spatial distribution $f_p(x, y, z)$ that is dictated by the emission profile of the particle in combination with the light diffraction in the microscope. Experimental factors, such as detector and sample properties, further influence the localization precision. The best localization precision theoretically achievable is given by the square root of the Cramér-Rao lower bound (CRLB), which is defined as the smallest possible variance any unbiased estimation algorithm can have[100]. The CRLB is given by the inverse of the diagonal terms of the Fisher information matrix, leading to

$$\sigma_x \geq \frac{1}{\sqrt{N\iiint_{-\infty}^{+\infty}\frac{1}{f_p(x,y,z)}\left(\frac{\partial f_p(x,y,z)}{\partial x}\right)^2 \mathrm{d}x\mathrm{d}y\mathrm{d}z}}$$

Similar expressions of the CRLB hold for the localization precision σ_y and σ_z corresponding to the position coordinates y_p and z_p, respectively. The reader is referred to the accompanying Review article of Small and Stahlheber[26] for more details on this topic. For an isotropic emitter in or close to the focal plane, the particle image that is determined by $f_p(x, y, z)$ is often approximated by a 2D Gaussian function[18]. Considering

only shot noise, the limit on the localization precision in this simple case[15,20] is given by

$$\sigma_x \geq \frac{s}{\sqrt{N}}$$

with N being the total number of detected photons and s the standard deviation of the Gaussian function. A similar expression of the CRLB holds for the localization precision σ_y. Besides shot noise, detector properties such as pixelation and readout noise can be included in the CRLB[15]. The limit on the localization precision outside the focal plane cannot be described by a simple analytical expression because 3D models of the particle image are substantially more complex.

If the algorithm that is used for the estimation of x_p is unbiased, the mean of its estimates approaches the true particle position with an increasing number of estimates n, i.e., $\bar{x}_p = x_p$. However, when the algorithm is biased, the mean $\bar{x}_p$ predicts the wrong position. Such an algorithm is called inaccurate, with a nonzero localization accuracy Δ_x on the x coordinate given by

$$\Delta_x = \bar{x}_p - x_p$$

Similar expressions of the localization accuracy hold for the position coordinates y_p and z_p. Because the localization accuracy does not involve individual measurements $x_{p,i}$, it is not sensitive to shot noise. However, the other factors that influence the localization precision—i.e., the spatial distribution of the photons in the image and the properties of the detector and sample—can in principle also affect the localization accuracy. Unlike the case of the localization precision, there is no fundamental limit on the achievable localization accuracy.
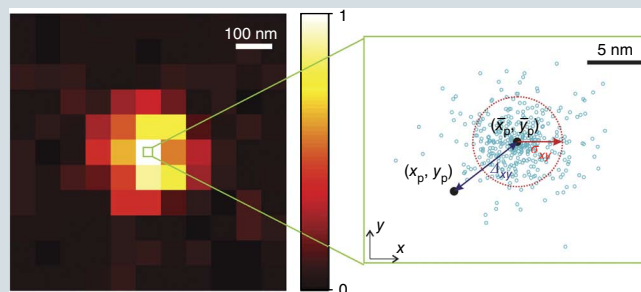

Figure 1 | Localization precision and accuracy. An example of an experimentally recorded image of a single emitter is shown. The real particle position (x_p, y_p) can be estimated from such an image with a lateral localization precision $\sigma_{xy} = (\sigma_x^2 + \sigma_y^2)^{1/2}$ and a lateral localization accuracy $\Delta_{xy} = (\Delta_x^2 + \Delta_y^2)^{1/2}$. The blue circles denote experimentally determined position estimates from different images of the same emitter, and $(\bar{x}_p, \bar{y}_p)$ is the average of these individual values.

appropriate readout wavelength, resulting in an image with spatially separated spots of light coming from each fluorophore. This allows the position of the activated fluorophores to be determined with a precision and accuracy smaller than the size of the PSF. Repeating the off-on cycle many times permits the position of many fluorophores in the sample to be determined. When structures are labeled with fluorophores at high enough density, and when a sufficient fraction of these labels are detected, a super-resolution image can be constructed from their estimated positions. The effective achievable resolution is therefore closely related to the localization precision and accuracy, so it is indispensable to have a clear understanding of how these parameters can be quantified and optimized. We will use localization microscopy to refer to any microscopy technique that relies on localizing individual fluorophores in order to generate images, whether they are part of a larger structure or not.

This Review provides an overview of recent work on localization precision and accuracy in relation to SPT and localization microscopy measurements, and it covers both theoretical considerations and practical issues to help users achieve the best localization precision and accuracy possible in their experiments. For information on the many other aspects of SPT and localization microscopy experiments, there are other excellent resources[10–13].

The influence of emitter properties

The location of a single emitter can be determined from its microscopy image using a specific algorithm, which we will refer to as the position estimator. Examples of such position estimators include fitting of a Gaussian function to the observed particle image and calculating its center of mass[14]. Whereas perfect localization accuracy can be achieved if the position estimator is unbiased, the localization precision can never be perfect because it is fundamentally limited by the Cramér-Rao lower bound (CRLB)[15] (**Box 1**). Both the precision and accuracy of position estimators depend on the shape of the emitter image, which is determined by the microscope optics and certain emitter properties. One important property is the spatial distribution of the photon emission, which is often implicitly assumed to be isotropic. However, a single fluorophore does not emit light in an isotropic fashion but rather behaves as an electric dipole[16]. This means that the shape of the emitter image can deviate substantially from the isotropic approximation, especially when there is limited or no rotation of the dipole during camera exposure, a fact that is increasingly being appreciated in the field of localization microscopy[17]. Another important emitter property that is mostly of relevance to SPT is motion during camera exposure time, which can distort the emitter image, whether the photons are emitted isotropically or not. Below we discuss several efforts that have been undertaken to theoretically describe the localization precision and sometimes accuracy for combinations of emitter properties and microscope optics that are typically encountered in SPT or localization microscopy. The most prominent theories are listed in **Figure 2**.

Isotropic emitters. In SPT and especially localization microscopy, the image of a single emitter is frequently approximated as a two-dimensional (2D) Gaussian function. This is reasonable for a conventional microscope setup in combination with the assumption of isotropic photon emission in or within a few hundred nanometers of the focal plane[18]. A popular position estimator is, therefore, fitting of a Gaussian function[14,19,20], as it is unbiased in this situation. Moreover, when a maximum-likelihood procedure is used, the localization precision can attain the CRLB[21]. In localization microscopy, which often has considerable background fluorescence, weighted least-square fitting may achieve similar localization precision, although in applications with low background fluorescence, such as in some SPT experiments, special treatment needs to be applied to pixels having weights approaching 0 at the edge of the particle image[21]. Unweighted least-squares fitting, also known as the Gaussian mask, does not have this problem, but it comes at the expense of a lower localization precision[20,21]. Another well-known position estimator in SPT and localization microscopy is the center-of-mass algorithm, whose localization precision and accuracy has been studied extensively in other contexts[22,23]. This position estimator is computationally fast[24], but experimental factors such as detector pixelation and background fluorescence will usually render it less precise[14] and accurate[22,25] than Gaussian fitting. Simple mathematical expressions have been derived that describe the localization precision and accuracy for Gaussian fitting and the center-of-mass algorithm (**Fig. 2**). Besides these position estimators, a range of other algorithms is available. The reader is referred to the accompanying Review by Small and Stahlheber[26] for more details on the computations that are involved in such position estimators.

As the distance of an isotropic emitter from the focal plane increases, the emitter image enlarges, resulting in an increase of the standard deviation of the fitted 2D Gaussian function (**Fig. 3a**). Although this means that the lateral localization precision decreases with increasing out-of-focus distance (**Box 1**), it has the advantage that the axial position can be estimated by fitting a Gaussian function with variable standard deviation[27]. The corresponding axial precision, however, strongly decreases with decreasing out-of-focus distance, essentially becoming 0 if the emitter is in the focal plane[28]. For an isotropic emitter further out of focus than a few hundred nanometers, the image exhibits a distinct pattern of diffraction rings (**Fig. 3b**). Because this diffraction ring pattern is unique to each axial position, a higher axial localization precision can be obtained than that near the focal plane. However, the estimation of the axial position can be accurate only when fitting a sufficiently elaborate theoretical 3D scalar[29] or vectorial[30,31] PSF model. Another option is to use a PSF model based on diffraction ring patterns from experimental images[32]. Theories on the localization precision that can be obtained with these complex position estimators are challenging to derive, and the performance is therefore usually compared to the CRLB in this situation (**Fig. 2**). Maximum-likelihood estimation of a scalar PSF model[29] has been shown to result in an axial localization precision that approaches the CRLB[33]. For emitters located at an increasing distance from the focal plane, the diffraction ring patterns gradually become unclear as the fluorescence signal becomes distributed over an increasingly large area, resulting in a concomitant deterioration of the localization precision. Indirectly determining the 3D position from the lateral shape of the particle image thus results in a highly nonuniform precision. Additionally, when there are no experimental complications such as a refractive index mismatch, it cannot be inferred from the lateral shape of the image whether the emitter is below or above the focal plane because the PSF is axially symmetric.

Recently, a variety of techniques have been developed to overcome these problems (**Box 2** and **Fig. 4**). One approach consists

Emitter properties	Microscope properties	Sample properties	Detector properties	Localization theory	Reference
Isotropic emitter	Conventional	Homogeneous background fluorescence	Pixelation & excess noise	σ_{xy} for Gaussian fitting	Eqs. (5) and (6) in Mortensen et al.[21]
			Pixelation & readout noise	σ_{xy} for center of mass	Eq. (17) in Li et al.[23]
				Δ_{xy} for center of mass	Eq. (6) in Berglund et al.[25]
				σ_z for Gaussian fitting	Eq. (5) in DeSantis et al.[28]
				CRLB on σ_{xy}	Ober et al.[15]
	Astigmatism, biplane, interference			CRLB on σ_{xy} and σ_z	von Middendorff et al.[38]
	Astigmatism, biplane, double helix		Pixelation	CRLB on σ_{xy} and σ_z	Badieirostami et al.[45]
	Conventional	Not accounted for	Pixelation & excess noise & readout noise	CRLB on σ_{xy}	Chao et al.[68]
			Pixelation	Δ_{xy} for center of mass	Eq. (12) in Jia et al.[22]
				CRLB on σ_z	Aguet et al.[33]
	Astigmatism, biplane, double helix			CRLB on σ_{xy} and σ_z	Grover et al.[52]
	Double helix			CRLB on σ_{xy} and σ_z	Pavani et al.[50]
Single-dipole emitter	Conventional	Homogeneous background fluorescence	Pixelation & excess noise	CRLB on σ_{xy}	Mortensen et al.[21]
			Pixelation	CRLB on σ_{xy}	Aguet et al.[56]
	Polarization imaging			CRLB on σ_{xy}	Stallinga et al.[58]
	Double helix and polarization imaging			CRLB on σ_{xy} and σ_z	Backlund et al.[59]
Ensemble of dipole emitters	Conventional	Homogeneous background fluorescence	Pixelation & excess noise	CRLB on σ_{xy}	Mortensen et al.[21]
Motion during camera exposure	Conventional	Homogeneous background fluorescence	Pixelation & excess noise	σ_{xy} for center of mass (diffusion)	Eq. (12) in Deschout et al.[64]
			Pixelation & readout noise	CRLB on σ_{xy} (linear and circular motion)	Wong et al.[63]

Figure 2 | Theories describing the localization precision or accuracy in SPT and localization microscopy. The table shows a non-exhaustive list of theories describing the lateral localization precision $\sigma_{xy} = (\sigma_x^2 + \sigma_y^2)^{1/2}$, the axial localization precision σ_z or the lateral localization accuracy $\Delta_{xy} = (\Delta_x^2 + \Delta_y^2)^{1/2}$. Each theory makes assumptions on the type of emitter, microscope, sample and detector. Although analytical expressions for the localization precision of simple estimators have been derived, for complicated estimators the localization precision performance is usually compared to the Cramér-Rao lower bound (CRLB).

of detecting the fluorescence the same emitter simultaneously in different imaging channels. In biplane (or multifocal-plane) microscopy, these channels each correspond to a different focal plane in the sample[34–36]. Comparison of the images allows unambiguous determination of the axial position over several micrometers and results in a fairly constant 3D localization precision[37,38]. In another technique, a mirror placed inside the sample adds an imaging channel corresponding to a side view of the normal front image, leading to almost isotropic 3D localization precision[39,40]. Sub-10-nm axial precision over a range of a few hundred nanometers around the focal plane has been obtained by combining the images of several channels produced by self-interference of the light emitted by a particle and collected by two opposing objectives[38,41,42].

In an alternative and more straightforward approach (**Box 2**), optical elements are placed in the detection beam path of a conventional

microscope setup to engineer a PSF that exhibits an axially dependent deformation. In this way, the shape of a single lateral image is unambiguously related to the axial position of the emitter. In one
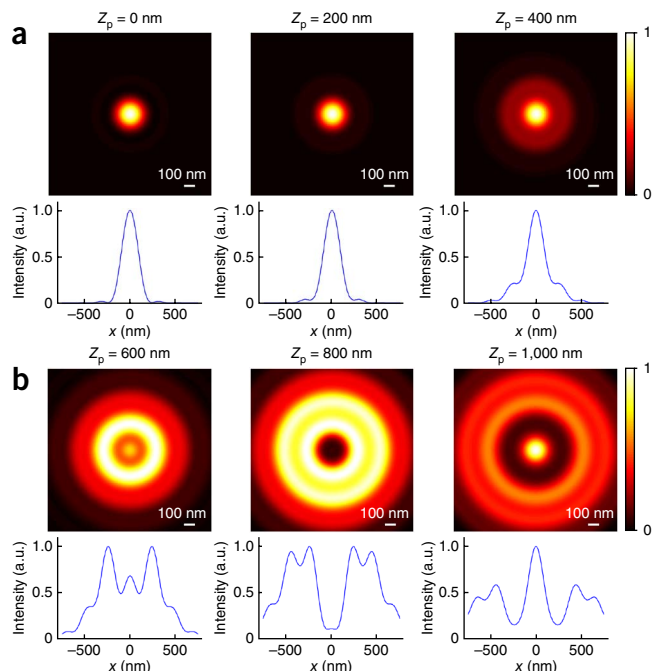
Figure 3 | Simulated images of an isotropic emitter at different axial positions Z_p and cross-sections through the emitter position along the x direction. (**a**) When the emitter is located within a few hundred nanometers from the focal plane ($Z_p = 0$ nm), the image can be approximated by a 2D Gaussian function with a standard deviation that slowly increases with the axial position. (**b**) For an isotropic emitter located further out of focus, the image exhibits a distinct pattern of diffraction rings that is unique to each axial position. The simulations in **a** and **b** were performed with an algorithm that is described elsewhere[98], assuming visible light ($\lambda = 550$ nm) and a high-NA objective lens (NA = 1.4). All images are normalized to their maximum values.

BOX 2 DETECTION SCHEMES FOR 3D LOCALIZATION

The lateral position of a particle can be readily derived from the location of its image recorded with a camera in a conventional optical microscope (**Fig. 4a**), but the axial position can only be deduced with highly variable precision from differences in the shape of its image at different distances from the focal plane. Special microscope setups have therefore been developed that allow unambiguous 3D localization with more uniform precision (**Fig. 4**). These setups rely on simultaneously recording multiple images of the same emitter via different detection beam paths and/or engineering of the 3D shape of the PSF.

A well-known technique that features multiple detection beam paths is biplane microscopy, in which a 50/50 beam splitter sends the light coming from a single emitter to two separate cameras or two separate regions of the same camera[34–36] (**Fig. 4b**). The two beam paths are designed to image two different planes in the sample, which allows axial particle localization through comparison of the two images. Increasing the number of image planes expands the axial localization range at the cost of localization precision.

In a setup similar to that of biplane microscopy, a mirror with a 45° angle to the optical axis is placed inside the sample to generate a side view of a single emitter in addition to the normal front view[39,40] (**Fig. 4c**). A 50/50 beam splitter sends the light coming from the emitter and its mirror image to two separate cameras (or two separate regions of a single camera). The lateral position is then determined from the front view of the emitter; the axial position, from the side view.

Imaging a particle through two opposing objective lenses in a 4Pi detection geometry[101] and analyzing the self-interference of the detected light allows determination of the axial position from the interference phase[38,41,42]. Unambiguously determining both phase and brightness of the light over at least one interference wave requires that a minimum of three images at different phase delays be recorded[42] (**Fig. 4d**). Depending on the axial emitter position, the optical path lengths are different, resulting in distinctive intensity ratios between the multiple emitter images.

Instead of detecting multiple images for each particle in separate beam paths, the axial position can be encoded in the 2D image of the particle by PSF engineering such as by placing a cylindrical lens in the beam path[43,44] (**Fig. 4e**). The introduced astigmatism generates elliptically shaped emitter images whose ellipticity and orientation depend on the axial particle position. The axial position can therefore be determined by
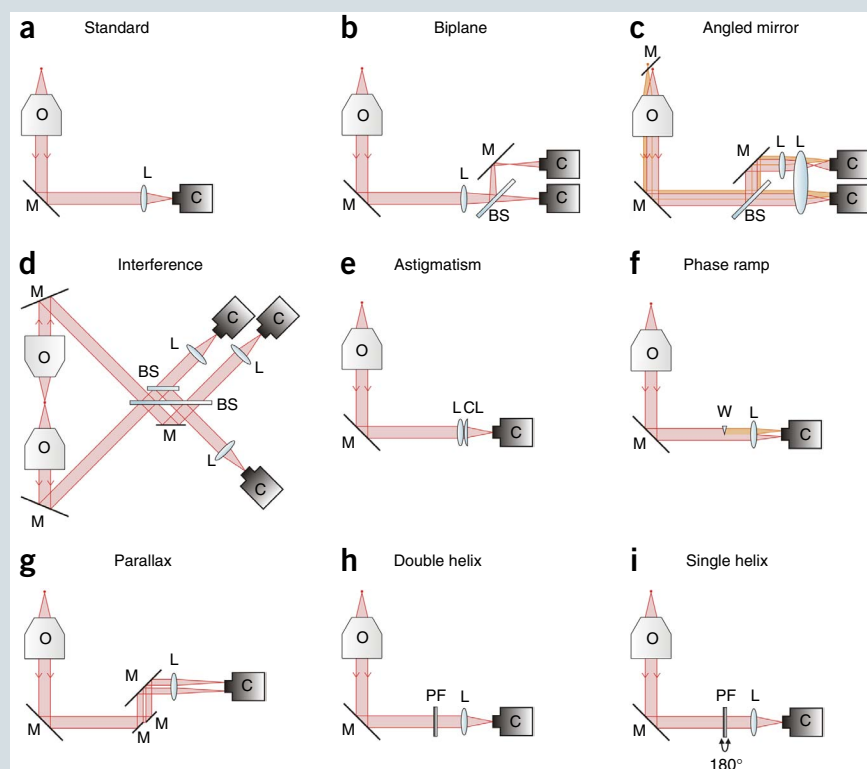

Figure 4 | Simplified illustrations of the detection beam path in several microscope setups that allow for 3D localization of single emitters. The main components in these setups are objective lenses (O), mirrors (M), beam splitters (BS), cameras (C), lenses (L), cylindrical lenses (CL), glass wedges (W) and phase filters (PF).

analyzing the shape of the particle image, and the lateral position is obtained from the image center.

Alternatively, a PSF can be engineered that splits each particle image into two lobes whose distance and/or relative orientation depend on the axial particle position. By introducing a phase ramp over one-half of the detection beam path with a glass wedge[46,47] (**Fig. 4f**) or by splitting the beam path in two by a pair of closely spaced nearly parallel mirrors[48] (**Fig. 4g**), a dual-lobe PSF can be produced where the axial position is determined from the distance between both lobes.

By using a phase filter, such as a spatial light modulator or manufactured phase plate, a more complex phase pattern can be generated. For a PSF in the shape of a double helix that rotates around the optical axis[50,51] (**Fig. 4h**), the axial position can be extracted from the relative orientation of the two lobes, and the midpoint between them describes the lateral position. Similarly, for a single helix (corkscrew)-shaped PSF that rotates around the optical axis[49] (**Fig. 4i**), the emitter can be localized by recording two images, one with the unmodified setup and another one with the phase filter rotated over 180°. The relative orientation between both images yields the axial position, and the midpoint between both represents the lateral position.

Figure 5 | Influence of dipole photon emission on localization precision and accuracy. (**a**) Simulated images of a dipole emitter for different dipole angles α in radians with the x axis at different axial positions Z_p. Some combinations of the dipole angle and axial position result in images that exhibit substantial asymmetry. Bottom, cross-sections of the images through the emitter position along the x direction. (**b**) Simulated images of a dipole emitter with dipole angle $\alpha = \pi/2$ at axial positions $Z_p = 0$ nm and $Z_p = 100$ nm that contain Poisson noise and pixelation. In each case, the fitted positions of 100 such images, as obtained from fitting of a 2D Gaussian function, are shown (blue dots) together with the actual position (red cross). A substantial lateral inaccuracy caused by the image asymmetry in case of $Z_p = 100$ nm is apparent. The simulations in **a** and **b** were performed with an algorithm that is described elsewhere[99], assuming visible light ($\lambda = 550$ nm) and a high-NA objective lens (NA = 1.4). All images are normalized to their maximum values.
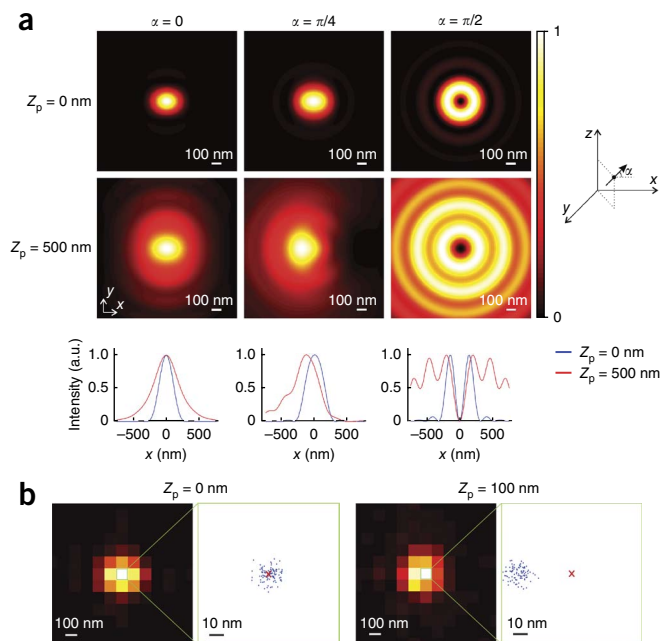
technique, a cylindrical lens is introduced, leading to an astigmatic particle image with changing ellipticity and orientation depending on the axial position[43,44]. This has been shown to result in a precision similar to that of the biplane approach, although less isotropic in three dimensions[37,45]. In another embodiment, a PSF consisting of two lobes whose relative distance depends on the axial position of the emitter is engineered by adding a prism over half the detection beam path, resulting in comparable precision to that in the astigmatic case[46,47]. In a technique called parallax, a similar effect is achieved by two closely spaced mirrors[48]. Alternatively, a phase filter can be used to engineer a single-helix[49] or double-helix[50,51] PSF, with the latter resulting in a 3D localization precision that is largely independent of the axial position over a range of several micrometers[45,52,53], more so than those for the astigmatism or multifocal-plane methods[45,52]. Further investigation is needed to find position estimators for these different 3D localization techniques that are unbiased and can attain the CRLB.

Single-dipole emitters. When a fluorophore is rigidly linked to a stationary structure, it can be rotationally immobile, resulting in a dipole that has a fixed orientation. Depending on this orientation, the image usually exhibits asymmetry that becomes more pronounced with increasing out-of-focus distance (**Fig. 5a**). This asymmetry can cause the intensity peak to be substantially displaced from the actual center of the dipole, resulting in lateral inaccuracies when using position estimators for isotropic emitters (**Fig. 5b**). It has been reported that, in the case of NA = 1.4, lateral displacements up to 100 nm can occur using the center-of-mass algorithm[54]. For lower values of the NA, this localization inaccuracy is typically several times smaller[17,55]. However, it should be kept in mind that the corresponding lower light collection efficiency (on the order of 60% for NA = 1.2 compared to NA = 1.4) reduces the localization precision. The fitting of a Gaussian function to the image of a dipole emitter has also been reported to introduce a lateral inaccuracy up to tens of nanometers[17,55]. One approach to avoid these localization inaccuracies is fitting of an image model that takes the dipole orientation into account[21,56]. However, this is quite challenging because different combinations of dipole orientation and out-of-focus distance can result in similar images. One solution comes from intensity-based measurement made with polarizing optics that allows determination of both lateral position and dipole orientation[57]. Combining this approach with fitting of an image model corrects for lateral inaccuracies induced by the dipole orientation[58]. Similarly, accurate 3D localization of dipole emitters has been

achieved by combining polarization optics with the double-helix PSF microscope setup[59]. Adapting other 3D localization techniques for dipole emitters could benefit the field as well.

Usually, a fluorophore will exhibit rotational motion dependent on the viscosity of the environment, the structure it is linked to and the nature of the linker moiety. As rotations take place over a time scale of a few nanoseconds[57,58], typical millisecond camera exposure times lead to images that can be described as coming from a superposition of fixed dipoles with random orientations in a certain angular range. Depending on the range of dipole orientations, localization inaccuracies of the order of 10 nm can occur with 2D Gaussian fitting[60]. Only in the extreme case of full rotational freedom, when the emitter image becomes symmetric, accurate position estimation is possible with 2D Gaussian fitting, with a precision approaching the CRLB[21,55]. An interesting topic for further investigation is the intermediate case between a fixed and a fast rotating dipole.

In conclusion, it is important to be aware of the substantial localization inaccuracies that can be present when labels are unable to rotate freely or when the localized molecules are not in focus. An effort to systematically study this effect for different labels and labeling strategies would be helpful to the localization microscopy community, as results suggest that many fluorescent proteins attached to molecules of interest do not have full rotational freedom, especially when attached to membrane-associated or cytoskeletal proteins[57]. In the meantime, users are advised to experimentally quantify the degree to which dipole orientation is isotropic in their system using a method that employs polarization optics[57]. Polarization anisotropy values reflect the degree to which the orientation is truly isotropic, with values close to 0 for dipoles that are able to sample all possible orientations within the camera exposure time. The anisotropies measured can be related roughly to the dipole angle accessible by the emitter using basic published anisotropy models[61].

Ensemble of dipole emitters. Nanoparticles or macromolecules having many fluorophores attached to them are often studied in SPT. Such an ensemble of fluorophores can be considered as a

BOX 3 SAMPLE ILLUMINATION IN SPT AND LOCALIZATION MICROSCOPY

There are different ways of illuminating the sample in SPT and localization microscopy experiments (**Fig. 8**). Wide-field or epifluorescence illumination (**Fig. 8a**) is easily obtained by focusing a light source along the optical axis in the back focal plane of the objective lens, generating a parallel light bundle in the sample. The major disadvantage of this type of illumination is that all planes above and below the focal plane also receive excitation light, resulting in a substantial amount of out-of-focus fluorescence. This background can strongly affect the localization precision and possibly the localization accuracy, especially in thick samples. To reduce these effects, various alternative illumination architectures exist to minimize the out-of-focus contribution.

One approach often used is total-internal-reflection fluorescence (TIRF) illumination[6,21] (**Fig. 8b**). Because the laser beam is focused off-center in the back focal plane of the objective lens, the light comes out of the objective lens at an angle such that it reflects off the interface between the coverslip and the sample, provided that the sample refractive index is smaller than that of the coverslip. This causes an evanescent wave to emerge in the sample over a couple of hundred nanometers so that only a small layer near the cover slip is illuminated. Although this approach strongly reduces the out-of-focus fluorescence, only the parts of the sample near the coverslip can be imaged.

Inclined (or oblique) illumination is a technique related to TIRF that is often used in SPT and localization microscopy[102,103] (**Fig. 8c**). The laser beam is also focused off-center in the back focal plane of the objective lens, but closer to the optical axis than in TIRF. This results in a light beam that comes out at a sharp angle. This light beam can have a thickness on the order of micrometers and therefore, just like TIRF, provides a superior contrast compared to wide-field illumination. By changing the off-center distance of the focused illumination beam in the back focal plane, the angle can be adjusted so as to illuminate the sample at different heights.

An approach that is starting to receive a lot of attention in localization microscopy and SPT is light-sheet illumination[78,104] (**Fig. 8d**). Unlike the previous techniques, the illumination is not provided by the detection objective lens but, in its most
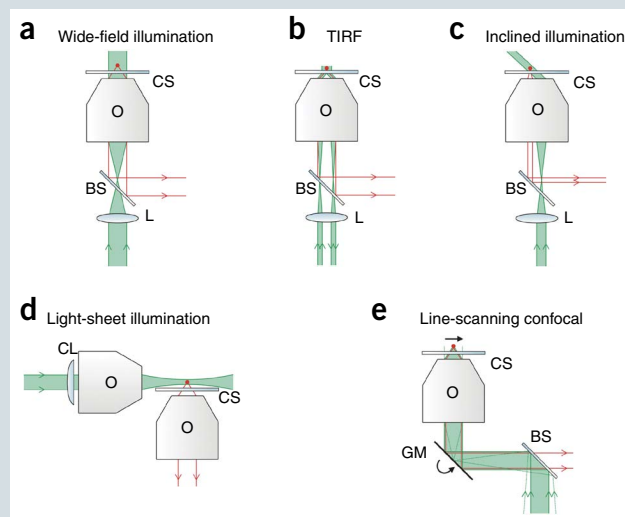

Figure 8 | Simplified illustrations of the illumination path in several microscope setups that allow for sample background reduction. The main components in these setups are objective lenses (O), beam splitters (BS), lenses (L), cylindrical lenses (CL), galvanometric mirrors (GM) and coverslips (CS).

common configuration, by the combination of a separate cylindrical lens and an illumination objective lens placed at a 90° angle to the detection path. Thus, a light sheet is generated that coincides with the focal plane of the detection objective lens. Although it is very difficult or even impossible to image the sample close to the coverslip, light-sheet illumination is an interesting approach for imaging in thick samples.

Confocal microscopy is another well-known technique to reduce out-of-focus fluorescence. A focused laser beam is scanned point by point through the focal plane in the sample, and the out-of-focus background is rejected by a pinhole in the detection beam path. Although confocal microscopy has not frequently been used for SPT or localization microscopy owing to a limited frame rate and/or sensitivity, one adaptation of the line-scanning confocal microscope has been reported that is capable of detecting single emitters[105] (**Fig. 8e**).

superposition of randomly oriented dipoles. Although its image is symmetric for wide-field illumination, this is not the case for total-internal-reflection fluorescence (TIRF) illumination (**Box 3**), as the electric field of TIRF light does not have a uniform orientation. Fitting of a Gaussian function to determine the lateral position is, therefore, slightly inaccurate in the case of TIRF. However, this lateral inaccuracy is identical for all emitters in the field of view[21], so the position estimates are accurate relative to each other. Stationary particles that are labeled with many fluorophores can, therefore, be approximated as isotropic emitters. An interesting topic for further investigation is the intermediary case of only a couple of fluorophores attached to a nanoparticle or macromolecule.

Translational motion during camera exposure. Until now, it was implicitly assumed that the emitter is stationary. However, translational

movement is commonly present in live samples and is by definition expected in SPT. When the distance traveled by the emitter during camera exposure reaches the same order of magnitude as that of the PSF width, the observed image can become substantially deformed (**Fig. 6a**) for Brownian motion. This in turn influences the localization precision and accuracy (**Fig. 6b**). The effect of linear and circular motion on lateral localization precision of isotropic emitters in focus has been investigated by determining the CRLB[62,63], which is of relevance for sample drift. However, particle motion at the microscopic scale more commonly exhibits a stochastic component. It has been shown that fitting of a 2D Gaussian function becomes inaccurate and imprecise in the case of substantial 3D diffusion during the camera exposure time[64]. The center-of-mass algorithm was shown to be a better choice for estimation of the lateral position in that case, as it does not depend on

Figure 6 | Influence of translational movement during camera exposure on localization precision and accuracy. (**a**) Simulated images of an isotropic emitter that is diffusing in the focal plane during a camera exposure time of 100 ms for different values of the diffusion coefficient D. The larger the value of D, the more the image is distorted. (**b**) Simulated images of a diffusing isotropic emitter with $D = 0.01$ µm²/s and $D = 1$ µm²/s that contain Poisson noise and pixelation. For both cases, a Brownian motion trajectory was simulated during the camera exposure time, and 100 images were simulated on the basis of the same Brownian trajectory but with independently added Poisson noise. Two exemplary images are shown. The positions obtained from fitting a 2D Gaussian function are shown (blue dots) together with the actual average position of the Brownian motion trajectory (red cross). A substantial decrease in precision and accuracy caused by the larger distortion of the image shape in the case of $D = 1$ µm²/s is apparent. The simulations in **a** and **b** were performed with an algorithm that is described elsewhere[64], assuming visible light ($\lambda = 550$ nm) and a high-NA objective lens (NA = 1.4). All images are normalized to their maximum intensity values.
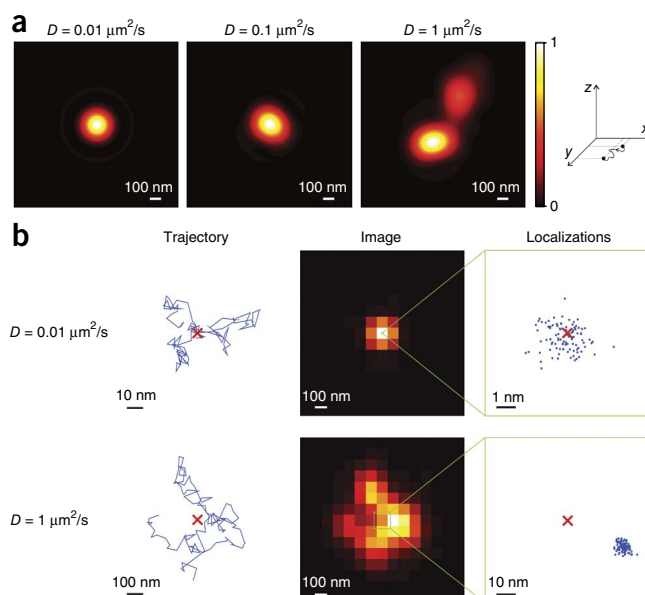
a particular shape of the emitter image[64]. When single molecules are tracked[65,66], the lateral inaccuracy due to molecular dipole orientation can be important if the fluorophore is unable to freely rotate within the camera exposure time. Further investigation is needed on the effect of translational motion on the localization precision and accuracy of dipole emitters, and on how motion influences precision and accuracy of 3D localization techniques.

The influence of experimental factors

The emitter image is only one factor that affects the precision and accuracy with which it can be localized. Just as important are the various properties of the detector and the sample, such as detector noise, sample drift and background fluorescence. When determining the localization precision and accuracy, it is thus crucial to properly account for all of these effects. This is required not only for correct optimization of the performance in localization microscopy and SPT but also for correct interpretation of the obtained data. Most theoretical descriptions of the localization precision and accuracy try to account for these properties to a certain extent (**Fig. 2**), and we discuss these below.

Detector. Several detector properties can affect the localization precision and accuracy. Detector pixelation limits the achievable localization precision because the location at which an individual photon arrives within the pixel area is unknown. Larger pixel sizes thus result in a reduced localization precision, which is considered by almost all theories (**Fig. 2**). However, the smaller the pixels are, the fewer photons are detected per pixel, which can result in detector noise overwhelming the signal.

Particularly for long exposure times, thermally induced 'dark current' that introduces a Poisson distributed background[15] can play an important role in charge-coupled device (CCD) and scientific complementary metal-oxide semiconductor (sCMOS) detectors, as it increases with the camera exposure time. For that reason, most high-end cameras nowadays are cooled, which results in dark current effectively being insignificant.

The CCD and, to a lesser extent, the sCMOS suffer from readout noise that follows a Gaussian distribution independent of the detected photon number. Although readout noise degrades the localization precision[15,62], it is usually not included in localization precision theories, arguably because the electron-multiplying CCD (EMCCD) has replaced the CCD in recent years.

The on-chip electron-multiplication process in these devices renders the readout noise effectively negligible. However, this process is also stochastic, which adds so-called excess noise to each pixel. In the case of high electron-multiplication levels (for example, 10^3), the pixel electrons after multiplication can still be described by a Poisson distribution, but with twice the variance[67]. This in turn decreases the localization precision by a factor of $\sqrt{2}$, although low light levels or low electron-multiplication values require a more complex treatment[21,68]. The reader is referred elsewhere for more detailed information on CCD and EMCCD properties that affect the localization precision[15,20,21].

The sCMOS has recently been explored as an alternative to the more expensive EMCCD. Its localization precision performance was found to be competitive with EMCCD for relatively high light levels, but it performs worse for very low light levels[69,70]. Unlike the EMCCD, the sCMOS can affect the localization accuracy because each pixel produces a unique amount of readout noise. This localization inaccuracy can be avoided by careful calibration of the readout noise pattern, in combination with a dedicated maximum likelihood–based position estimator[71].

Another source of potential localization inaccuracies is the nonuniform sensitivity of the pixels over the detector area[72]. The so-called photoresponse nonuniformity is caused by differences in the conversion efficiency of photons to electrons between pixels or even within the same pixel, leading to a nonuniform image even when all pixels are illuminated uniformly. This can lead to localization inaccuracies on the order of nanometers, especially when the nonuniformities have the same scale as the width of the particle image. This localization inaccuracy can be corrected for by mapping the photoresponse nonuniformity in detail: for example, by recording the image of an illuminated pinhole that is scanned across the pixels with subpixel step size[72].

Sample drift. Sample drift on the nanometer scale is hard to avoid as it can be caused by a variety of sources, such as vibration and mechanical relaxation of the microscope. Drift during camera exposure affects the localization precision and accuracy in a way that is similar to (linear) particle motion, and it also negatively influences SPT and localization microscopy data analysis. In the

Figure 7 | Experimental images illustrating the effect of sample background on the localization precision. (**a**) Images of fluorescent subresolution objects at different axial positions z_p are localized by means of an astigmatic PSF (see **Box 2**) in a transparent agarose gel (thin sample) and in a 100-μm-diameter cellular spheroid (thick sample). (**b**) The axial localization precision can be determined as the full-width at half-maximum (FWHM$_z$) (see **Box 1**) of the distribution of repeatedly measured axial positions $z_{p,i}$ of subresolution objects subtracted by the corresponding mean of the measured axial positions, $\bar{z}_p$. The experimental value of the axial localization precision in the agarose gel is FWHM$_z$ = 68 nm, and this value increases to FWHM$_z$ = 141 nm (i.e., localization precision decreases) deep within the cellular spheroid.

context of the latter issue, one often-reported drift correction approach is to relate all position estimates to the position of a fiduciary marker embedded in the sample[6,8]. As thermal motion of the markers can distort drift correction, it is better to attach them to the coverslip instead[73,74]. To maintain a good precision of the location estimates, researchers should use a fiduciary marker bright enough such that its location can be determined with a precision much better than the localization precision of the tracked particles or imaged single molecules. For that reason, bright fluorescent beads are often chosen[8]. However, if such a bright structure is located too close to the particle of interest, it may add to its background, in effect reducing the localization precision, or it might be so bright that it saturates the detector. A better solution is to use a bright fiduciary marker, close to the particle of interest, that fluoresces in a spectrally separate channel[73]. Techniques for drift correction that do not require the addition of fiduciary markers rely on the use of spatial correlation between subsequent super-resolution images[43,75,76] or the use of structures of the sample itself (for example, intracellular structures that are imaged separately but simultaneously with transmitted light) as fiduciary markers[77]. However, these methods do not work if the structures of interest are dynamic.

Sample background. Sample background, coming from out-of-focus fluorescence or autofluorescence, can substantially reduce the localization precision and, for estimators such as the center-of-mass algorithm, also the localization accuracy[25]. This is especially the case when the particles are located deep inside thick biological samples. The extra background inside cellular spheroids of 100-μm diameter has been shown to lead to a decrease in precision by a factor of 2 compared to the ideal situation without background[78] (**Fig. 7**). Homogeneous background fluorescence is often incorporated in the precision and accuracy theories (**Fig. 2**). It takes the form of a Poisson-distributed background and is thus equivalent to dark current. In some samples, especially thick ones, the background fluorescence can be heterogeneous, introducing localization inaccuracies up to tens of nanometers (**Supplementary Fig. 1** and **Supplementary Note 1**). Although image processing procedures can be used to filter out background heterogeneity to some extent, a complete correction is difficult to achieve. Background from out-of-focus fluorescence should be avoided by confining the illumination as much as possible to the portion of the sample that is in focus, using a microscope setup with a suitable illumination configuration (**Box 3** and **Fig. 8**).

PSF deformation. The PSF can become deformed because of refractive-index variations in the sample, light scattering or absorption, and refractive-index mismatch between the sample, embedding medium and coverslip. This results in a deformation
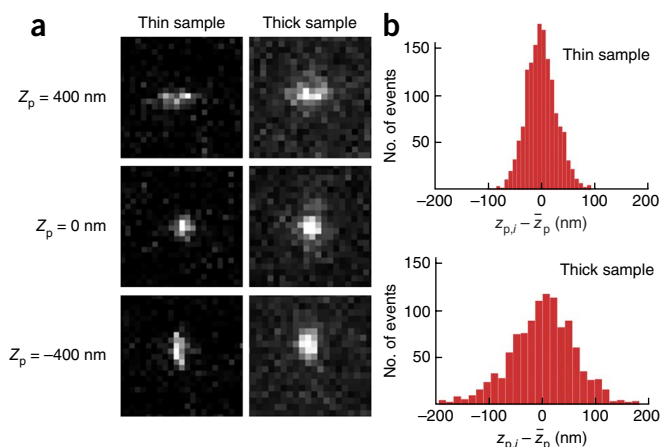
of the emitter image that becomes more pronounced with deeper focusing into the sample. Lateral displacement of the PSF caused by comatic aberrations can be especially problematic, to an extent depending on the axial position of the emitter[74]. Accurate position estimation can be achieved only by fitting an experimentally determined emitter image model[43,74]. These experimental particle-reference images can be obtained from an independently recorded z stack of a fluorescent nonblinking particle, such as a fluorescent bead. Possible differences in photobleaching[34,37], refractive-index mismatch[43,79,80] or dipole orientation[81] between the actual image and the calibration stack need to be corrected for. Recently, an interesting possibility for at least partially mitigating these complications has been reported, wherein an image model is derived from only a couple of experimental images at different z positions using a phase-retrieval algorithm[82]. Another approach that is worthwhile to explore is adaptive optics, as it has already been shown useful in removing PSF deformations caused by optical inhomogeneity in the sample[83].

Label displacement. Because the fluorescent label is usually not identical to the molecule of interest, the determined emitter position in any SPT or localization microscopy experiment is displaced with respect to the real molecule position. One type of label displacement arises from the finite size of the fluorescent label itself. Although irrelevant for single fluorophores with a diameter of about 1 nm, a displacement on the order of tens of nanometers arises by using nanoparticles such as quantum dots or fluorescent beads. A second important source of displacement comes from any linker moiety used to attach the label to the target molecule. For instance, the combination of primary and secondary antibodies can introduce displacements of 10–20 nm. Nanobodies[84] and aptamers[85] could be a better option in this regard because their size is on the order of nanometers. One should also be aware that the linker moiety might restrict the rotational freedom of the fluorescent label and result in localization inaccuracies that exceed the label displacement[60]. For a discussion on the classes of labels that are suitable for localization microscopy, see **Box 4**.

Measuring the localization precision

For the case of isotropic emitters near the focal plane, simple mathematical expressions can be derived that describe the localization precision obtained with a certain position estimator (**Fig. 2**). However, estimator-specific localization precision theories are challenging to derive for more complicated situations—for example,

BOX 4   TYPES OF LABELS FOR LOCALIZATION MICROSCOPY

A number of options exist for labeling samples for localization microscopy. For a comprehensive overview of suitable labels, the reader is referred elsewhere[106–108]. Here, the advantages and disadvantages of the three main classes of fluorescent labels (fluorescent proteins, organic dyes and quantum dots) are discussed.

Photoactivatable and photoswitchable fluorescent proteins (PAFPs) offer the convenience of genetic control of the fluorophore, attachment to a protein of interest and controlled subcellular localization and expression level. Furthermore, their moderate size (a cylindrical shape of diameter ~2.8 nm and length ~4 nm) and their compatibility with the cellular milieu make them advantageous for live- and fixed-cell imaging. As a matter of fact, the first live-cell localization microscopy study used PAFPs[109]. It is advised to use monomeric forms of PAFPs to minimize self-aggregation[110]. A downside in comparison to organic dyes is that PAFPs generally emit fewer photons before photobleaching[106]. The turnover rate and the potential for problems induced by PAFP overexpression are also crucial considerations that can limit the density of labeled molecules and ultimately the image quality and achieved resolution.

Conventional organic dyes may be used for localization microscopy provided that proper conditions can be obtained such that the majority of fluorophores are within long-lived dark states. Conditions that achieve this requirement have been determined for a large number of such probes and often require the presence of thiol or other reducing agents within the imaging buffer[106]. Their small size and the relatively large number of photons they can emit make organic dyes advantageous for applications in which maximization of localization precision and accuracy is desired. In that case it is better to attach organic dyes to small molecules (such as phalloidin), rather than to large antibodies, for targeting to specific biological structures. In addition, antibody labeling is mostly limited to fixed permeabilized cells. Although live-cell applications are possible in which molecules on the cell exterior are labeled, the introduction of thiol or other reducing agents can affect live-cell physiology.

Caged organic dyes are another option for labeling cells, the advantages of which are similar to other organic dyes, but without the requirement for reducing agents or thiol. With respect to both conventional and caged organic dyes, recently developed methods to couple these probes to small genetically encoded binding sites that can be expressed in cells have enabled live- and fixed-cell labeling schemes that offer many of the advantages of both PAFPs and organic dyes (i.e., Snap-tags[81], 'click' chemistry[111] or HaloTags[112]), although background can be a problem[108].

Quantum dots are also an option for cell labeling; these have the advantage of high brightness and resistance to photobleaching[113] but are also prone to self-aggregation[114] and blinking[115]. Quantum dots have recently been synthesized with sizes as small as a few nanometers[116] but so far have not been produced in a photoactivatable or photoconvertible form, although blinking has been exploited to allow super-resolution imaging[117]. The density of quantum dots in the on state, unlike the density of PAFPs or organic dyes, is thus hard to control by illumination, limiting their use to applications in which small populations of quantum dots attached to molecules of interest are visualized over long periods of time. Methods to label both extracellular and intracellular structures using quantum dots in fixed cells, and to some extent in live cells, have been developed[108]. However, the delivery of quantum dots to the cytosol of living cells[118] and attenuating their cytotoxicity remain challenging. Thus, although there are many options, the best choice of label will depend very much upon the type of localization microscopy application.

---

in the case of emitters with a fixed dipole orientation or the case of PSF deformations—and instead the performance is usually compared to the CRLB (**Fig. 2**). Therefore, if at all possible, it is preferable to determine the actual localization precision experimentally. For stationary emitters (i.e., without translational movement), as is often the case in localization microscopy, this can be done by acquiring a series of images of a sparse set of emitters. By determining the location of the same emitter in subsequent images, the standard deviation on the localization can be determined, which is by definition the localization precision (**Box 1**). As this procedure is sensitive to instrumental drift, it is better to determine the precision from the distance between consecutive positions rather than the positions themselves[20]. For determining the effective localization precision of particles that are moving during the camera exposure time, as that is typically the case for SPT experiments, a method was recently reported that makes use of two simultaneously acquired images by introducing a 50/50 beam splitter or dichroic mirror in the detection path[64].

Implication for localization microscopy and SPT
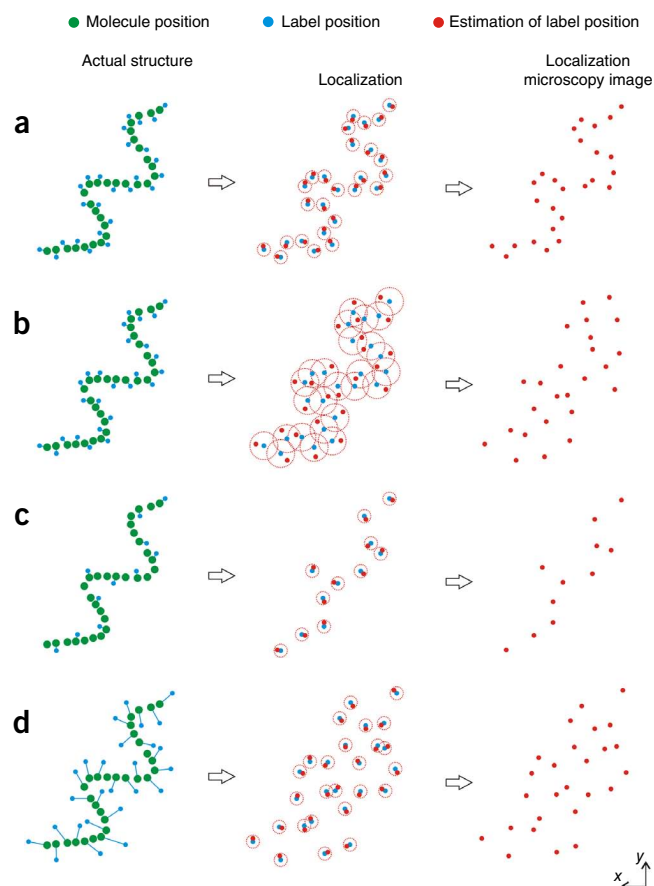**Resolution in localization microscopy.** The two parameters that most commonly limit the resolution in localization microscopy are localization precision and label density (**Figs. 9** and **10**), but so far there has been little consensus in the field on how resolution should be reported and measured. One of the first attempts to replace the conventional theory of Abbe[1] and Rayleigh[2] in the context of localization microscopy was called the fundamental resolution measure[86]. In this framework, the resolution of an optical microscope is completely determined by the localization precision (**Figs. 9a,b** and **10a**). However, this is generally not sufficient to describe the resolution in localization microscopy images, as it does not account for the effect of label density[87] (**Figs. 9a,c** and **10b**). Often, the following two guidelines are considered: if a desired resolution is to be obtained, then (i) the localization precision value should evidently be smaller and (ii) the nearest-neighbor distance between localized fluorophores (in the final rendered image) within the structure of interest should not be larger than half the desired resolution. Note that the resolution in other super-resolution microscopy techniques is governed by similar guidelines. For instance, it was recently reported that the resolution in stimulated emission depletion microscopy images equally depends on the label density[85].

Of course, there are circumstances in which these guidelines do not work well. Guideline (ii) is an analogy of the Nyquist criterion, stating that the characteristic distance between two neighboring

Figure 9 | Influence of localization precision, label density and label displacement on the resolution in a localization microscopy image. (**a**–**d**) The actual structure consisting of molecules is symbolized by the green dots. The apparent structure that is observed in the localization microscopy image consists of estimated positions (red dots) of the labels (blue dots). The open red circles represent the localization precision. (**a**) The localization microscopy image faithfully represents the actual structure only when the localization precision and label density are sufficiently high and the label displacement is sufficiently small. The resolution in the localization microscopy images is decreased by lower localization precision (**b**), lower label density (**c**) and higher label displacement (**d**).

emitters must be smaller than half of the smallest sample feature that can be resolved[81,88]. However, it has recently been shown that the Nyquist criterion can overestimate the increase of resolution with label density[89]. In the case of a sample with a small number of molecules of interest—for example, a membrane receptor normally expressed at the level of a few hundred copies per cell—the structure itself does not have continuous boundaries. Localizing every molecule of interest with arbitrarily high precision will still yield an image that appears sparse, which means that guideline (ii) does not apply. Image resolution is thus arguably not a meaningful concept in this particular case. The kind of structure being examined also plays a role in the reliability of the information obtained. For example, confirming a gap in a filament imaged by localization microscopy requires that the labeling of this filament be as uniform as possible, and even if this is achieved, the stochasticity of the localization process will cause 'false' gaps to occur by chance. The only way to interpret such an image is to compare the width and frequency of observed gaps with the width and frequency of gaps expected by chance.

Thus, guidelines (i) and (ii) do not account for all of the sources of resolution degradation, and ideally a more sophisticated estimate of resolution should be made. One example of a general estimator of image information and resolution is the information transfer function derived from Fisher information theory[90], which quantifies the total amount of information captured within a localization microscopy image and includes the effects of localization precision and density. However, the practical use of this theoretical framework might be limited, as it requires a prior model of the sample structure. A different approach that does allow one to estimate the resolution directly from the recorded localization microscopy image, accounting for both localization precision and label density, is based on the calculation of the Fourier ring correlation (FRC)[91,92]. An extension of this concept was shown to capture the effect of line-like (such as microtu-

bule[92]) and ring-like (such as nuclear pore complex[91]) sample features on the resolution. However, the usefulness of the FRC for determining whether structures with many other particular geometries (for example, two globular objects or a gap in a filament) are resolved remains to be investigated. In addition it would seem that the FRC is not relevant for structures without continuous boundaries. Thus, for the near future, the best practice is probably for users to report both measured localization precision and localized probe density (or nearest-neighbor distance) for each rendered image, even if a sophisticated resolution measure such as the FRC is calculated.

Several approaches have been used to experimentally characterize the resolution in localization microscopy. Often, this is done purely qualitatively by imaging known structures, such as actin filaments or microtubules (**Fig. 10** and **Supplementary Note 2**). Quantitative measurements of resolution have also been reported using nanoscale rulers, i.e., structures that contain single emitters at predefined distances from each other. For instance, double-stranded DNA labeled with multiple emitters separated by a fixed number of base pairs has been used as a nanoscale ruler[8]. A more rigid and controllable nanoscale ruler has recently been obtained by DNA origami, using short fluorescently labeled DNA staple strands that bind at particular points on a long single-stranded
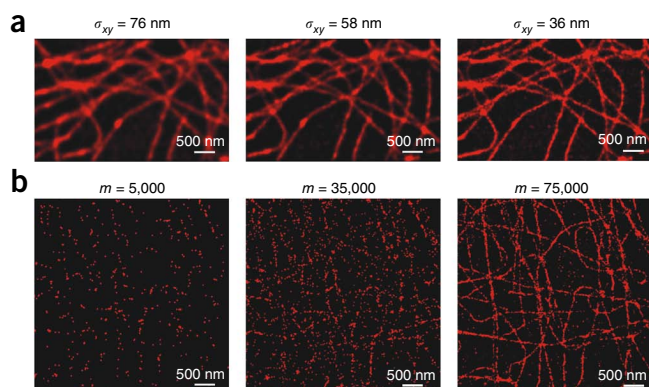

Figure 10 | Experimental images illustrating the influence of localization precision and label density on the resolution in localization microscopy. Microtubules in HeLa cells labeled with Alexa 647 are shown. (**a**,**b**) The images show the effect of an increasing localization precision (i.e., decreasing values of the lateral localization precision σ_{xy}) (**a**) and an increasing labeling density (i.e., increasing values of the number of localized molecules m) (**b**). See **Supplementary Note 2** for more information.
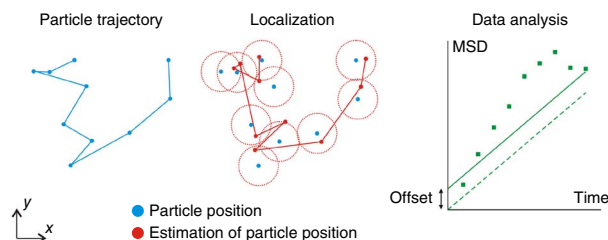
Figure 11 | Influence of localization precision on the analysis of single-particle trajectories in the case of Brownian motion. The observed trajectory (red line) consisting of estimated particle positions (red dots) is different from the actual trajectory (blue line) consisting of actual particle positions (blue dots) because of the limited localization precision (symbolized by the open red circles). The observed mean-square displacements (MSD) of the observed trajectory (green squares) as a function of the time lags in the trajectory can be modeled by a linear function (green line) with an offset value that is related to the localization precision.

DNA scaffold[93]. However, such measurements should be interpreted with care, as they are relevant only when the localization precision, labeling density and geometry are all comparable to those of the actual sample. Simulated images are a better alternative because they allow easier control over these three parameters. For instance, by taking the measured localization precision and label density from an experiment, it is possible to simulate images of emitters on structures with different geometries. Comparison of the simulated and experimental images allows better understanding of what structures have been resolved.

Not only localization imprecision but also inaccuracy can adversely affect the resolution in localization microscopy. When induced by dipole orientations or detector photoresponse nonuniformities, inaccuracy can in principle be eliminated by application of the best practices for these situations. Localization inaccuracy induced by the labeling method poses more of a problem (**Fig. 9a,d**) and thus warrants further investigation. This is also the case for emitter photoblinking[94], which can affect the apparent label density and, therefore, the resolution.

SPT analysis. In SPT, the measured trajectories of nanoparticles or macromolecules are usually analyzed to obtain information about the particle mobility or its interaction with the surrounding medium. For correct trajectory analysis it is crucial to account for any nonzero localization precision or accuracy. A popular type of analysis is the fitting of a theoretical model to the mean-square displacements of the trajectories[11,13,95]. For instance, the mean-square displacement is linearly proportional to the time lag between the observed locations in the case of free Brownian motion, whereas typically a power law is considered in the case of anomalous diffusion[95]. The effect of limited localization precision has to be included in the model through a constant offset[5,96] (**Fig. 11**). In the context of SPT, where particles or molecules are typically mobile, motion during camera exposure and its effect on localization precision has to be taken into account. Surprisingly, it was not until recently that this effect was considered for free Brownian motion[64,97]; more efforts are still required for other motion types.

Conclusion and future outlook
Localization microscopy and SPT have provided invaluable insight into biological systems at the nanoscale. As these powerful techniques are becoming more mature and are being applied to increasingly complex biological systems, it is of crucial importance to fully understand localization precision and accuracy of single emitters, two related concepts that are at the heart of these techniques. This means that the use of popular position estimators, such as fitting an isotropic Gaussian, should be used with consideration, as they yield optimal localization precision and accuracy only in circumstances that are in fact rarely achieved in SPT or localization microscopy experiments. Continuation of the ongoing efforts to investigate the localization precision and accuracy of a whole array of other position estimators will be of great help in selecting the most suitable position estimator for a given situation. Furthermore, as SPT is being used to probe nanoscale motion with increasing temporal resolution, effects due to nonzero localization precision and accuracy should be taken into account in the analysis of SPT data. In localization microscopy, it will be crucial to develop a correct understanding of spatial resolution in biological samples in relation to localization precision and accuracy.

Note: Any Supplementary Information and Source Data files are available in the online version of the paper.

COMPETING FINANCIAL INTERESTS
The authors declare competing financial interests: details are available in the online version of the paper.

Reprints and permissions information is available online at http://www.nature.com/reprints/index.html.

1. Abbe, E. Beiträge zur Theorie des Mikroskops und der mikroskopischen Wahrnehmung. *Arch. Mikroskop. Anat.* **9**, 413–418 (1873).
2. Rayleigh, L. On the theory of optical images, with special reference to the microscope. *Philos. Mag.* **42**, 167–195 (1896).
3. McCutchen, C.W. Superresolution in microscopy and the Abbe resolution limit. *J. Opt. Soc. Am.* **57**, 1190–1192 (1967).
4. Toraldo di Francia, G. Resolving power and information. *J. Opt. Soc. Am.* **45**, 497–499 (1955).
5. Crocker, J.C. & Grier, D.G. Methods of digital video microscopy for colloidal studies. *J. Colloid Interface Sci.* **179**, 298–310 (1996).
6. Betzig, E. *et al.* Imaging intracellular fluorescent proteins at nanometer resolution. *Science* **313**, 1642–1645 (2006).
   This is one of the three studies that introduced super-resolution localization microscopy based on localizing single fluorophores. This strongly increased the interest in understanding and optimizing localization precision and accuracy.
7. Hess, S.T., Girirajan, T.P.K. & Mason, M.D. Ultra-high resolution imaging by fluorescence photoactivation localization microscopy. *Biophys. J.* **91**, 4258–4272 (2006).
8. Rust, M.J., Bates, M. & Zhuang, X.W. Sub-diffraction-limit imaging by stochastic optical reconstruction microscopy (STORM). *Nat. Methods* **3**, 793–796 (2006).
9. Hell, S.W. Microscopy and its focal switch. *Nat. Methods* **6**, 24–32 (2009).
10. Gould, T.J., Verkhusha, V.V. & Hess, S.T. Imaging biological structures with fluorescence photoactivation localization microscopy. *Nat. Protoc.* **4**, 291–308 (2009).
11. Levi, V. & Gratton, E. Exploring dynamics in living cells by tracking single particles. *Cell Biochem. Biophys.* **48**, 1–15 (2007).
12. van de Linde, S. *et al.* Direct stochastic optical reconstruction microscopy with standard fluorescent probes. *Nat. Protoc.* **6**, 991–1009 (2011).
13. Wieser, S. & Schütz, G.J. Tracking single molecules in the live cell plasma membrane—do's and don'ts. *Methods* **46**, 131–140 (2008).

14. Cheezum, M.K., Walker, W.F. & Guilford, W.H. Quantitative comparison of algorithms for tracking single fluorescent particles. *Biophys. J.* **81**, 2378–2388 (2001).

15. Ober, R.J., Ram, S. & Ward, E.S. Localization accuracy in single-molecule microscopy. *Biophys. J.* **86**, 1185–1200 (2004).
    This study reports on the maximum achievable localization precision, assuming isotropic photon emission and a CCD detector, using the concept of the Cramér-Rao lower bound.

16. Bartko, A.P. & Dickson, R.M. Imaging three-dimensional single molecule orientations. *J. Phys. Chem. B* **103**, 11237–11241 (1999).

17. Enderlein, J., Toprak, E. & Selvin, P.R. Polarization effect on position accuracy of fluorophore localization. *Opt. Express* **14**, 8111–8120 (2006).
    This study shows that the popular fitting of a 2D Gaussian function can introduce a localization inaccuracy up to tens of nanometers for fluorophores with a fixed dipole orientation.

18. Zhang, B., Zerubia, J. & Olivo-Marin, J.C. Gaussian approximations of fluorescence microscope point-spread function models. *Appl. Opt.* **46**, 1819–1829 (2007).

19. Bobroff, N. Position measurement with a resolution and noise-limited instrument. *Rev. Sci. Instrum.* **57**, 1152–1157 (1986).

20. Thompson, R.E., Larson, D.R. & Webb, W.W. Precise nanometer localization analysis for individual fluorescent probes. *Biophys. J.* **82**, 2775–2783 (2002).
    This study introduced a simple formula that describes the localization precision of the popular fitting of a 2D Gaussian function, assuming isotropic photon emission and a CCD detector. The formula was later adjusted by others.

21. Mortensen, K.I., Churchman, L.S., Spudich, J.A. & Flyvbjerg, H. Optimized localization analysis for single-molecule tracking and super-resolution microscopy. *Nat. Methods* **7**, 377–381 (2010).
    This extensive study describes the localization precision of different position estimators, assuming either isotropic or dipole photon emission and either a CCD or EMCCD detector. The maximum-likelihood procedure is shown to approach the maximum achievable localization precision.

22. Jia, H., Yang, J.K. & Li, X.J. Minimum variance unbiased subpixel centroid estimation of point image limited by photon shot noise. *J. Opt. Soc. Am. A Opt. Image Sci. Vis.* **27**, 2038–2045 (2010).

23. Li, H., Song, H., Rao, C. & Rao, X. Accuracy analysis of centroid calculated by a modified center detection algorithm for Shack-Hartmann wavefront sensor. *Opt. Commun.* **281**, 750–755 (2008).

24. Abraham, A.V., Ram, S., Chao, J., Ward, E.S. & Ober, R.J. Quantitative study of single molecule location estimation techniques. *Opt. Express* **17**, 23352–23373 (2009).

25. Berglund, A.J., McMahon, M.D., McClelland, J.J. & Liddle, J.A. Fast, bias-free algorithm for tracking single particles with variable size and shape. *Opt. Express* **16**, 14064–14075 (2008).

26. Small, A. & Stahlheber, S. Fluorophore localization algorithms for super-resolution microscopy. *Nat. Methods* **11**, 267–279 (2014).

27. van Oijen, A.M., Köhler, J., Schmidt, J., Müller, M. & Brakenhoff, G.J. 3-Dimensional super-resolution by spectrally selective imaging. *Chem. Phys. Lett.* **292**, 183–187 (1998).

28. DeSantis, M.C., Zareh, S.K., Li, X.L., Blankenship, R.E. & Wang, Y.M. Single-image axial localization precision analysis for individual fluorophores. *Opt. Express* **20**, 3057–3065 (2012).

29. Frisken Gibson, S. & Lanni, F. Experimental test of an analytical model of aberration in an oil-immersion objective lens used in three-dimensional light-microscopy. *J. Opt. Soc. Am. A* **8**, 1601–1613 (1991).

30. Richards, B. & Wolf, E. Electromagnetic diffraction in optical systems. II. Structure of the image field in an aplanatic system. *Proc. R. Soc. Lond. A Math. Phys. Sci.* **253**, 358–379 (1959).

31. Török, P., Varga, P., Laczik, Z. & Booker, G.R. Electromagnetic diffraction of light focused through a planar interface between materials of mismatched refractive indexes: an integral representation. *J. Opt. Soc. Am. A Opt. Image Sci. Vis.* **12**, 325–332 (1995).

32. Speidel, M., Jónás, A. & Florin, E.L. Three-dimensional tracking of fluorescent nanoparticles with subnanometer precision by use of off-focus imaging. *Opt. Lett.* **28**, 69–71 (2003).

33. Aguet, F., Van De Ville, D. & Unser, M. A maximum-likelihood formalism for sub-resolution axial localization of fluorescent nanoparticles. *Opt. Express* **13**, 10503–10522 (2005).

34. Juette, M.F. *et al.* Three-dimensional sub–100 nm resolution fluorescence microscopy of thick samples. *Nat. Methods* **5**, 527–529 (2008).

35. Prabhat, P., Ram, S., Ward, E.S. & Ober, R.J. Simultaneous imaging of different focal planes in fluorescence microscopy for the study of cellular dynamics in three dimensions. *IEEE Trans. Nanobioscience i* **3**, 237–242 (2004).

36. Toprak, E., Balci, H., Blehm, B.H. & Selvin, P.R. Three-dimensional particle tracking via bifocal imaging. *Nano Lett.* **7**, 2043–2045 (2007).

37. Mlodzianoski, M.J., Juette, M.F., Beane, G.L. & Bewersdorf, J. Experimental characterization of 3D localization techniques for particle-tracking and super-resolution microscopy. *Opt. Express* **17**, 8264–8277 (2009).

38. von Middendorff, C., Egner, A., Geisler, C., Hell, S. & Schönle, A. Isotropic 3D nanoscopy based on single emitter switching. *Opt. Express* **16**, 20774–20788 (2008).

39. McMahon, M.D., Berglund, A.J., Carmichael, P., McClelland, J.J. & Liddle, J.A. 3D particle trajectories observed by orthogonal tracking microscopy. *ACS Nano* **3**, 609–614 (2009).

40. Tang, J., Akerboom, J., Vaziri, A., Looger, L.L. & Shank, C.V. Near-isotropic 3D optical nanoscopy with photon-limited chromophores. *Proc. Natl. Acad. Sci. USA* **107**, 10068–10073 (2010).

41. Aquino, D. *et al.* Two-color nanoscopy of three-dimensional volumes by 4Pi detection of stochastically switched fluorophores. *Nat. Methods* **8**, 353–359 (2011).

42. Shtengel, G. *et al.* Interferometric fluorescent super-resolution microscopy resolves 3D cellular ultrastructure. *Proc. Natl. Acad. Sci. USA* **106**, 3125–3130 (2009).

43. Huang, B., Wang, W.Q., Bates, M. & Zhuang, X.W. Three-dimensional super-resolution imaging by stochastic optical reconstruction microscopy. *Science* **319**, 810–813 (2008).
    This study is one of the first to use an engineered PSF in the context of localization microscopy to improve the axial localization precision. The authors used astigmatism to encode the axial position of the emitter in the PSF shape.

44. Kao, H.P. & Verkman, A.S. Tracking of single fluorescent particles in three dimensions: use of cylindrical optics to encode particle position. *Biophys. J.* **67**, 1291–1300 (1994).

45. Badieirostami, M., Lew, M.D., Thompson, M.A. & Moerner, W.E. Three-dimensional localization precision of the double-helix point spread function versus astigmatism and biplane. *Appl. Phys. Lett.* **97**, 161103 (2010).

46. Baddeley, D., Cannell, M. & Soeller, C. Three-dimensional sub-100 nm super-resolution imaging of biological samples using the objective pupil. *Nano Res.* **4**, 589–598 (2011).

47. Yajima, J., Mizutani, K. & Nishizaka, T. A torque component present in mitotic kinesin Eg5 revealed by three-dimensional tracking. *Nat. Struct. Mol. Biol.* **15**, 1119–1121 (2008).

48. Sun, Y., McKenna, J.D., Murray, J.M., Ostap, E.M. & Goldman, Y.E. Parallax: high accuracy three-dimensional single molecule tracking using split images. *Nano Lett.* **9**, 2676–2682 (2009).

49. Lew, M.D., Lee, S.F., Badieirostami, M. & Moerner, W.E. Corkscrew point spread function for far-field three-dimensional nanoscale localization of pointlike objects. *Opt. Lett.* **36**, 202–204 (2011).

50. Pavani, S.R.P. & Piestun, R. Three dimensional tracking of fluorescent microparticles using a photon-limited double-helix response system. *Opt. Express* **16**, 22048–22057 (2008).

51. Thompson, M.A., Lew, M.D., Badieirostami, M. & Moerner, W.E. Localizing and tracking single nanoscale emitters in three dimensions with high spatiotemporal resolution using a double-helix point spread function. *Nano Lett.* **10**, 211–218 (2010).

52. Grover, G., Pavani, R.P. & Piestun, R. Performance limits on three-dimensional particle localization in photon-limited microscopy. *Opt. Lett.* **35**, 3306–3308 (2010).

53. Pavani, S.R.P., Greengard, A. & Piestun, R. Three-dimensional localization with nanometer accuracy using a detector-limited double-helix point spread function system. *Appl. Phys. Lett.* **95**, 021103 (2009).

54. Engelhardt, J. *et al.* Molecular orientation affects localization accuracy in superresolution far-field fluorescence microscopy. *Nano Lett.* **11**, 209–213 (2011).

55. Stallinga, S. & Rieger, B. Accuracy of the Gaussian point spread function model in 2D localization microscopy. *Opt. Express* **18**, 24461–24476 (2010).

56. Aguet, F., Geissbühler, S., Märki, I., Lasser, T. & Unser, M. Super-resolution orientation estimation and localization of fluorescent dipoles using 3-D steerable filters. *Opt. Express* **17**, 6829–6848 (2009).

57. Gould, T.J. *et al.* Nanoscale imaging of molecular positions and anisotropies. *Nat. Methods* **5**, 1027–1030 (2008).

58. Stallinga, S. & Rieger, B. Position and orientation estimation of fixed dipole emitters using an effective Hermite point spread function model. *Opt. Express* **20**, 5896–5921 (2012).

59. Backlund, M.P. *et al.* Simultaneous, accurate measurement of the 3D position and orientation of single molecules. *Proc. Natl. Acad. Sci. USA* **109**, 19087–19092 (2012).

60. Lew, M.D., Backlund, M.P. & Moerner, W.E. Rotational mobility of single molecules affects localization accuracy in super-resolution fluorescence microscopy. *Nano Lett.* **13**, 3967–3972 (2013).

61. Lakowicz, J.R. *Principles of Fluorescence Spectroscopy* 3rd edn. (Springer, 2006).

62. Ram, S., Ward, E.S. & Ober, R.J. A stochastic analysis of performance limits for optical microscopes. *Multidimens. Syst. Signal Process.* **17**, 27–57 (2006).

63. Wong, Y., Lin, Z. & Ober, R.J. Limit of the accuracy of parameter estimation for moving single molecules imaged by fluorescence microscopy. *IEEE Trams. Signal Process.* **59**, 895–911 (2011).

64. Deschout, H., Neyts, K. & Braeckmans, K. The influence of movement on the localization precision of sub-resolution particles in fluorescence microscopy. *J. Biophotonics* **5**, 97–109 (2012).

65. Manley, S. *et al.* High-density mapping of single-molecule trajectories with photoactivated localization microscopy. *Nat. Methods* **5**, 155–157 (2008).

66. Yildiz, A. *et al.* Myosin V walks hand-over-hand: single fluorophore imaging with 1.5-nm localization. *Science* **300**, 2061–2065 (2003).

67. Hynecek, J. & Nishiwaki, T. Excess noise and other important characteristics of low light level imaging using charge multiplying CCDs. *IEEE Trans. Electron Devices* **50**, 239–245 (2003).

68. Chao, J., Ward, E.S. & Ober, R.J. Fisher information matrix for branching processes with application to electron-multiplying charge-coupled devices. *Multidimens. Syst. Signal Process.* **23**, 349–379 (2012).

69. Huang, Z.L. *et al.* Localization-based super-resolution microscopy with an sCMOS camera. *Opt. Express* **19**, 19156–19168 (2011).

70. Quan, T., Zeng, S. & Huang, Z.-L. Localization capability and limitation of electron-multiplying charge-coupled, scientific complementary metal-oxide semiconductor, and charge-coupled devices for superresolution imaging. *J. Biomed. Opt.* **15**, 066005 (2010).

71. Huang, F. *et al.* Video-rate nanoscopy using sCMOS camera-specific single-molecule localization algorithms. *Nat. Methods* **10**, 653–658 (2013).

72. Pertsinidis, A., Zhang, Y.X. & Chu, S. Subnanometre single-molecule localization, registration and distance measurements. *Nature* **466**, 647–651 (2010).

73. Lee, S.H. *et al.* Using fixed fiduciary markers for stage drift correction. *Opt. Express* **20**, 12177–12183 (2012).

74. York, A.G., Ghitani, A., Vaziri, A., Davidson, M.W. & Shroff, H. Confined activation and subdiffractive localization enables whole-cell PALM with genetically expressed probes. *Nat. Methods* **8**, 327–333 (2011).

75. Geisler, C. *et al.* Drift estimation for single marker switching based imaging schemes. *Opt. Express* **20**, 7274–7289 (2012).

76. Mlodzianoski, M.J. *et al.* Sample drift correction in 3D fluorescence photo-activation localization microscopy. *Opt. Express* **19**, 15009–15019 (2011).

77. Mennella, V. *et al.* Subdiffraction-resolution fluorescence microscopy reveals a domain of the centrosome critical for pericentriolar material organization. *Nat. Cell Biol.* **14**, 1159–1168 (2012).

78. Cella Zanacchi, F. *et al.* Live-cell 3D super-resolution imaging in thick biological samples. *Nat. Methods* **8**, 1047–1049 (2011).

79. Deng, Y. & Shaevitz, J.W. Effect of aberration on height calibration in three-dimensional localization-based microscopy and particle tracking. *Appl. Opt.* **48**, 1886–1890 (2009).

80. Huang, B., Jones, S.A., Brandenburg, B. & Zhuang, X.W. Whole-cell 3D STORM reveals interactions between cellular structures with nanometer-scale resolution. *Nat. Methods* **5**, 1047–1052 (2008).

81. Jones, S.A., Shim, S.-H., He, J. & Zhuang, X. Fast, three-dimensional super-resolution imaging of live cells. *Nat. Methods* **8**, 499–505 (2011).

82. Quirin, S., Pavani, S.R.P. & Piestun, R. Optimal 3D single-molecule localization for superresolution microscopy with aberrations and engineered point spread functions. *Proc. Natl. Acad. Sci. USA* **109**, 675–679 (2012).

83. Ji, N., Milkie, D.E. & Betzig, E. Adaptive optics via pupil segmentation for high-resolution imaging in biological tissues. *Nat. Methods* **7**, 141–147 (2010).

84. Ries, J., Kaplan, C., Platonova, E., Eghlidi, H. & Ewers, H. A simple, versatile method for GFP-based super-resolution microscopy via nanobodies. *Nat. Methods* **9**, 582–584 (2012).

85. Opazo, F. *et al.* Aptamers as potential tools for super-resolution microscopy. *Nat. Methods* **9**, 938–939 (2012).

86. Ram, S., Ward, E.S. & Ober, R.J. Beyond Rayleigh's criterion: a resolution measure with application to single-molecule microscopy. *Proc. Natl. Acad. Sci. USA* **103**, 4457–4462 (2006).

87. Gould, T.J., Hess, S.T. & Bewersdorf, J. Optical nanoscopy: from acquisition to analysis. *Annu. Rev. Biomed. Eng.* **14**, 231–254 (2012).

88. Shroff, H., Galbraith, C.G., Galbraith, J.A. & Betzig, E. Live-cell photoactivated localization microscopy of nanoscale adhesion dynamics. *Nat. Methods* **5**, 417–423 (2008).

89. Fitzgerald, J.E., Lu, J. & Schnitzer, M.J. Estimation theoretic measure of resolution for stochastic localization microscopy. *Phys. Rev. Lett.* **109**, 048102 (2012).

90. Mukamel, E.A. & Schnitzer, M.J. Unified resolution bounds for conventional and stochastic localization fluorescence microscopy. *Phys. Rev. Lett.* **109**, 168102 (2012).

91. Banterle, N., Bui, K.H., Lemke, E.A. & Beck, M. Fourier ring correlation as a resolution criterion for super-resolution microscopy. *J. Struct. Biol.* **183**, 363–367 (2013).

92. Nieuwenhuizen, R.P.J. *et al.* Measuring image resolution in optical nanoscopy. *Nat. Methods* **10**, 557–562 (2013).
This study reports on a practical measure to calculate the resolution in localization microscopy images based on FRC, taking into account the localization precision, among other factors.

93. Steinhauer, C., Jungmann, R., Sobey, T.L., Simmel, F.C. & Tinnefeld, P. DNA origami as a nanoscopic ruler for super-resolution microscopy. *Angew. Chem. Int. Ed. Engl.* **48**, 8870–8873 (2009).

94. Annibale, P., Vanni, S., Scarselli, M., Rothlisberger, U. & Radenovic, A. Quantitative photo activated localization microscopy: unraveling the effects of photoblinking. *PLoS ONE* **6**, e22678 (2011).

95. Saxton, M.J. & Jacobson, K. Single-particle tracking: applications to membrane dynamics. *Annu. Rev. Biophys, Biomol. Struct.* **26**, 373–399 (1997).

96. Savin, T. & Doyle, P.S. Static and dynamic errors in particle tracking microrheology. *Biophys. J.* **88**, 623–638 (2005).

97. Michalet, X. Mean square displacement analysis of single-particle trajectories with localization error: Brownian motion in an isotropic medium. *Phys. Rev. E* **82**, 041914 (2010).
This detailed study describes the effect of the localization imprecision on the analysis of the mean-square displacements of trajectories that are obtained by SPT experiments.

98. Kirshner, H., Aguet, F., Sage, D. & Unser, M. 3-D PSF fitting for fluorescence microscopy: implementation and localization application. *J. Microsc.* **249**, 13–25 (2013).

99. Hanser, B.M., Gustafsson, M.G.L., Agard, D.A. & Sedat, J.W. Phase-retrieved pupil functions in wide-field fluorescence microscopy. *J. Microsc.* **216**, 32–48 (2004).

100. Winick, K.A. Cramér-Rao lower bounds on the performance of charge-coupled-device optical position estimators. *J. Opt. Soc. Am. A* **3**, 1809–1815 (1986).

101. Bewersdorf, J., Schmidt, R. & Hell, S.W. Comparison of I^{5}M and 4Pi-microscopy. *J. Microsc.* **222**, 105–117 (2006).

102. Giannone, G. *et al.* Dynamic superresolution imaging of endogenous proteins on living cells at ultra-high density. *Biophys. J.* **99**, 1303–1310 (2010).

103. Tokunaga, M., Imamoto, N. & Sakata-Sogawa, K. Highly inclined thin illumination enables clear single-molecule imaging in cells. *Nat. Methods* **5**, 159–161 (2008).

104. Ritter, J.G., Veith, R., Veenendaal, A., Siebrasse, J.P. & Kubitscheck, U. Light sheet microscopy for single molecule tracking in living tissue. *PLoS ONE* **5**, e11639 (2010).

105. Lee, J., Miyanaga, Y., Ueda, M. & Hohng, S. Video-rate confocal microscopy for single-molecule imaging in live cells and superresolution fluorescence imaging. *Biophys. J.* **103**, 1691–1697 (2012).

106. Dempsey, G.T., Vaughan, J.C., Chen, K.H., Bates, M. & Zhuang, X.W. Evaluation of fluorophores for optimal performance in localization-based super-resolution imaging. *Nat. Methods* **8**, 1027–1036 (2011).

107. Lippincott-Schwartz, J. & Patterson, G.H. Photoactivatable fluorescent proteins for diffraction-limited and super-resolution imaging. *Trends Cell Biol.* **19**, 555–565 (2009).

108. Xu, J. *et al.* Labeling cytosolic targets in live cells with blinking probes. *J. Phys. Chem. Lett.* **4**, 2138–2146 (2013).

109. Hess, S.T. *et al.* Dynamic clustered distribution of hemagglutinin resolved at 40 nm in living cell membranes discriminates between raft theories. *Proc. Natl. Acad. Sci. USA* **104**, 17370–17375 (2007).

110. Zacharias, D.A., Violin, J.D., Newton, A.C. & Tsien, R.Y. Partitioning of lipid-modified monomeric GFPs into membrane microdomains of live cells. *Science* **296**, 913–916 (2002).

111. Zessin, P.J.M., Finan, K. & Heilemann, M. Super-resolution fluorescence imaging of chromosomal DNA. *J. Struct. Biol.* **177**, 344–348 (2012).

112. Los, G.V. *et al.* HaloTag: a novel protein labeling technology for cell imaging and protein analysis. *ACS Chem. Biol.* **3**, 373–382 (2008).

113. Chan, W.C.W. & Nie, S.M. Quantum dot bioconjugates for ultrasensitive nonisotopic detection. *Science* **281**, 2016–2018 (1998).

114. Rochira, J.A. *et al.* Fluorescence intermittency limits brightness in CdSe/ZnS nanoparticles quantified by fluorescence correlation spectroscopy. *J. Phys. Chem. C* **111**, 1695–1708 (2007).

115. Kuno, M., Fromm, D.P., Hamann, H.F., Gallagher, A. & Nesbitt, D.J. Nonexponential "blinking" kinetics of single CdSe quantum dots: a universal power law behavior. *J. Chem. Phys.* **112**, 3117–3120 (2000).

116. Chen, W., Wang, Z., Lin, Z. & Lin, L. Absorption and luminescence of the surface states in ZnS nanoparticles. *J. Appl. Phys.* **82**, 3111–3115 (1997).

117. Lidke, K.A., Rieger, B., Jovin, T.M. & Heintzmann, R. Superresolution by localization of quantum dots using blinking statistics. *Opt. Express* **13**, 7052–7062 (2005).

118. Delehanty, J.B., Mattoussi, H. & Medintz, I.L. Delivering quantum dots into cells: strategies, progress and remaining issues. *Anal. Bioanal. Chem.* **393**, 1091–1105 (2009).